Materials Characterization 112 (2016) 134–141

Contents lists available at ScienceDirect

Materials Characterization

journal homepage: www.elsevier.com/locate/matchar

The effect of phase transformation in the plastic zone on the hydrogen-assisted fatigue crack growth of 301 stainless steel

T.C. Chen [b], S.T. Chen [a], W. Kai [a], L.W. Tsay [a,*]

[a] Institute of Materials Engineering, National Taiwan Ocean University, Keelung 20224, Taiwan, ROC
[b] Institute of Nuclear Energy Research, Division of Nuclear Fuels and Materials, Lungtan, Taoyuan 32546, Taiwan, ROC

ARTICLE INFO

Article history:
Received 9 July 2015
Received in revised form 11 December 2015
Accepted 15 December 2015
Available online 17 December 2015

Keywords:
Stainless steel
Fatigue crack growth rate
Hydrogen embrittlement
Martensite

ABSTRACT

The effects of rolling and stress ratio (R) on the fatigue crack growth rates (FCGRs) of AISI 301 stainless steel (SS) in gaseous hydrogen were investigated. Accelerated fatigue crack growth occurred for the solution-annealed (SA) and cold rolled (CR) specimens tested in gaseous hydrogen, and especially for the CR specimen at high R. Moreover, a sufficiently high ΔK and/or Kmax were required to activate hydrogen-assisted fatigue crack growth of the 301 SS. Fatigue crack growth within a narrow α′ martensite layer was responsible for the rapid FCGRs of the specimens in hydrogen. The plastic zone size, identified by hardness distributions, was much larger than the region that underwent phase transformation.

1. Introduction

Austenitic stainless steels (SSs) have good corrosion resistance and moderate mechanical properties, so they are often used as structural materials in industrial applications. Metastable austenitic SSs may undergo phase transformation from austenite to ferromagnetic α′-martensite during plastic deformation [1–4]. Angel [5] suggested the use of the Md_{30} temperature to evaluate the stability of austenitic SSs. Higher Md_{30} temperatures clearly represent less stable alloys. It has been reported that the region beneath the crack surface of a fatigued 321 SS contains strain-induced martensite at the intersections of slip bands [6]. The induced martensite is reported to reduce fatigue crack growth rates (FCGRs) and increase the threshold stress intensity for crack growth [7]. However, in hydrogen-containing environments, the formation of martensite leads to increased FCGRs [8–16], which is particularly evident in unstable austenitic SSs as compared with stable austenitic SSs [15–18].

A suitable amount of cold work can lower the stress corrosion cracking (SCC) susceptibility of austenitic SSs, whereas an excessive cold work reverses the trend [19,20]. In addition, the pitting potential of 304L SS determined in 0.1 N NaCl solution decreases with up to 50% cold work, but it increases beyond 50% [3]. It has been pointed out that the work-hardened layer in both the machined and grounded 304L SS, which is accompanied with a high volume fraction of martensite, is highly prone to SCC [21]. However, the hydrogen-assisted fatigue crack growth of rolled austenitic SSs has attracted little attention in the literature [22–24]. Accordingly, this study investigated the influence of rolling and stress ratio on the fatigue crack growth behavior of AISI 301 SS in air and hydrogen. The fracture features of the tested samples were examined with a scanning electron microscope (SEM). The variation in FCGRs of the specimens in hydrogen was correlated with the change in fracture features and metallurgical variables. An electron backscatter diffraction (EBSD) map has previously been used to assess the damage induced by low-cycle fatigue [25]. In this study, the EBSD was used to distinguish the phase constituents around the crack tip of selected specimens. Moreover, the plastic zone size ahead of the crack tip of the fatigued specimen was estimated by hardness distributions and compared with the phase transformation zone identified by the EBSD map.

2. Material and experimental procedures

The chemical composition (wt.%) of the AISI 301 SS used in this study was as follows: 16.71 Cr, 6.89 Ni, 0.08 C, 1.16 Mn, 0.54 Si, 0.02 P, 0.003 S, and a balance of Fe. The 301 SS was received in a solution-annealed (SA) condition in plate form with a thickness of 4.5 mm. The SA specimen was rolled to a final thickness of 3.6 mm (20% reduction in thickness) at room temperature. The corresponding specimens were designated as CR (cold-rolled). All the specimens were fatigue-strained at the thickness of 3.6 mm.

Fatigue crack growth tests were conducted on a computerized MTS closed-loop, servo-controlled hydraulic testing system at room temperature, using wire-cut compact tension (CT) specimens according to the ASTM E647 standard (Fig. 1). Fatigue tests were performed under a constant-amplitude sinusoidal-waveform loading cycle with a

* Corresponding author.
E-mail address: b0186@mail.ntou.edu.tw (L.W. Tsay).

http://dx.doi.org/10.1016/j.matchar.2015.12.016
1044-5803/

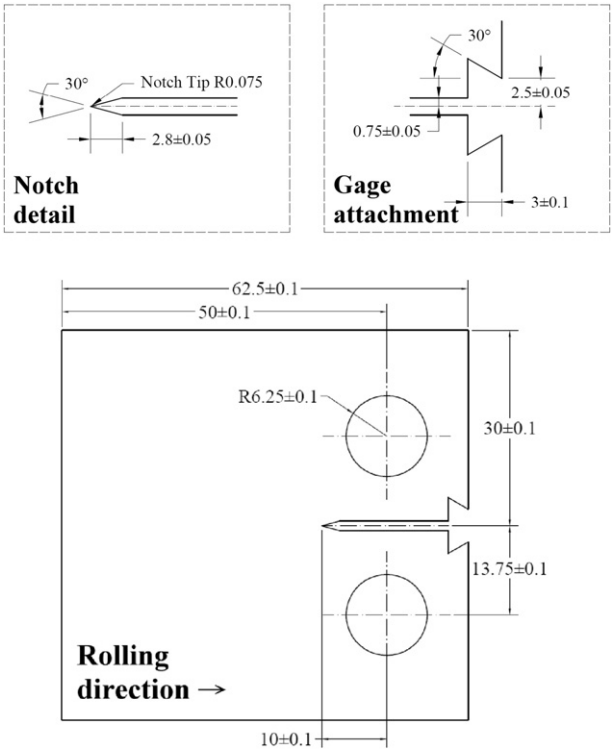

Fig. 1. Schematic dimensions of the compact tension (CT) specimens (unit: mm).

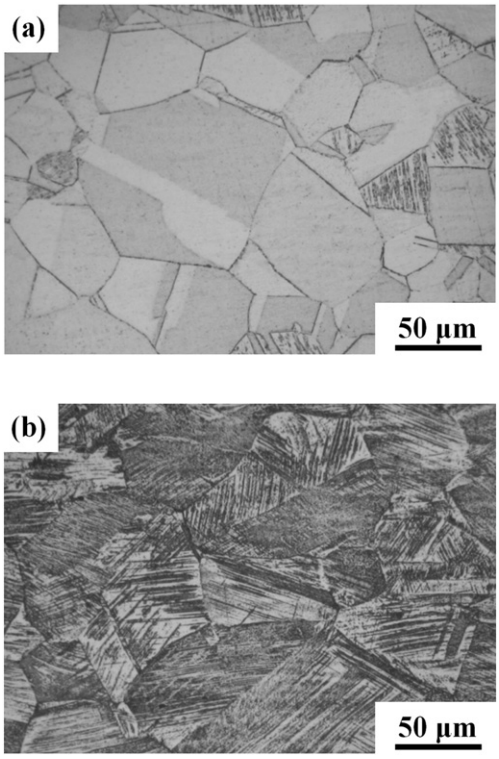

Fig. 2. Optical microstructures of the (a) SA and (b) CR specimens in the T–L (fatigue crack growth) direction.

frequency of 20 Hz. Moreover, the stress ratio (R) was maintained at either 0.1 or 0.5. Crack length was determined by the compliance function proposed by Saxena and Hudak [26] and confirmed by 30× optical microscopy. In addition to CT specimens tested in air, the influence of hydrogen embrittlement on the FCGRs of the specimens was evaluated by testing specimens inside a stainless steel chamber charged with gaseous hydrogen at a pressure of 0.2 MPa. The CR specimens fatigue-tested in air and in hydrogen were designated as the CR-a and CR-h specimens, respectively. The results presented are typical examples of repeated experimental data of at least three tests.

In order to determine the hardness distribution within an area of 4.8 × 4.8 mm ahead of a fatigue crack tip, an automatic Vickers hardness tester was applied with a load of 100 gf for 15 s. For every 80 μm depth in the selected area, indentation was performed once automatically using the crack route as the symmetrical centerline: i.e., about 3600 points were measured. The amount of strain-induced α′-martensite in various specimens was determined with a Ferritescope, which measures the volume fraction of strained-induced α′-martensite in the detected site [27,28]. The phase constituents on the fatigue-cracked surface of the specimen were determined by X-ray diffraction (XRD) using MoKα radiation. Moreover, the α′ (bcc)- and ε (hcp)-martensite along with γ-austenite (fcc) were also inspected using EBSD to locate their distributions adjacent to the fatigue crack. The macro-fracture appearance and the detailed fracture features of various specimens were examined with a Hitachi 4800 scanning electron microscope (SEM).

3. Results

3.1. Microstructural observations and ferrite measurements

Fig. 2 compares the optical microstructures of the rolled specimens to those of the SA specimen. The microstructure of the SA specimen was composed primarily of equiaxial grains with some twins inside (Fig. 2(a)), whereas dense basket-weaved slip bands were found in the CR specimen (Fig. 2(b)). The surface hardness of the SA specimen was about HV 190, but that of the CR specimen was as high as HV 480. Measurements of the ferrite content (α′-martensite, ferromagnetic phase) were made on bulk materials before fatigue tests. The results indicated that the ferrite content of the CR specimen was 19.1%, but no ferrite was detected in the SA specimen. Therefore, a noticeable surface-hardening after rolling was associated with the great amount of strain-induced martensite that formed in the specimen. The yield strength of the SA and CR specimens was 228 and 826 MPa, respectively. The yield strength of the CR specimen was much higher than that of the SA specimen. In contrast, after cold rolling, the elongation dropped from 70% to 31%. This meant that the introduction of phase transformation and numerous dislocations into the CR specimen impeded the dislocations motion with a concomitant decrease in ductility.

3.2. Fatigue crack growth tests

Fig. 3 shows the fatigue crack growth behavior of the SA and CR specimens tested either in air or in hydrogen at two stress ratios. Regardless of the specimen conditions, increasing the stress ratio raised the FCGRs as a whole over the testing ΔK range in air. Crack growth in the SA and CR specimens tested in hydrogen was significantly faster than that in counterpart specimens tested in air. It was noticed that gaseous hydrogen embrittlement had little effect on accelerating crack growth of the SA specimen in the threshold ΔK range at R = 0.1. The threshold ΔK range was about 14.1 MPa$\sqrt{m}$ or Kmax of 15.6 MPa$\sqrt{m}$ at R = 0.1. When the stress ratio was increased to 0.5, hydrogen-assisted fatigue crack growth occurred even in the low ΔK range (9.7 MPa$\sqrt{m}$ or Kmax of 19.4 MPa$\sqrt{m}$). It was deduced that hydrogen could be driven to the crack tip to induce cracking/embrittlement under sufficiently high applied stress/Kmax. Applying the stress/Kmax beneath the threshold condition, local hydrogen embrittlement might not assist crack growth in a ductile material.

Fig. 4 compares the fatigue crack growth behaviors of CR specimens tested in air or gaseous hydrogen to that of the SA specimens. In air (Fig. 4(a)), the CR specimen had higher FCGRs than the SA specimen